HOKKAIDO UNIVERSITY

Title	Breaking of unsteady lee waves generated by diurnal tides
Author(s)	Nakamura, T.; Isoda, Y.; Mitsudera, H. et al.
Citation	Geophysical Research Letters, 37, L04602 https://doi.org/10.1029/2009GL041456
Issue Date	2010-02-20
Doc URL	https://hdl.handle.net/2115/43790
Rights	Copyright 2010 by the American Geophysical Union
Type	journal article
File Information	GRL37_L04602.pdf

Click Here
for
Full
Article

Breaking of unsteady lee waves generated by diurnal tides

T. Nakamura,[1] Y. Isoda,[2] H. Mitsudera,[1] S. Takagi,[3] and M. Nagasawa[4]

[1] Diapycnal mixing caused through breaking of large-amplitude internal lee waves generated by sub-inertial diurnal tides, which are modulated with a 18.6-year period, is hypothesized to be fundamental to both the intermediate-layer ventilation and the bi-decadal oscillation around the North Pacific Ocean. The first observational evidence of such wave breaking is presented here. The breaking wave observed had ~200 m height and ~1 km width, and its associated diapycnal mixing was estimated to be ~1.5 m^2 s^{-1}, with a temporal average ~10^4 times larger than typical values in the open oceans. Our estimate suggests that a similar mixing process occurs globally, particularly around the Pacific and Antarctic Oceans. **Citation:** Nakamura, T., Y. Isoda, H. Mitsudera, S. Takagi, and M. Nagasawa (2010), Breaking of unsteady lee waves generated by diurnal tides, *Geophys. Res. Lett.*, *37*, L04602, doi:10.1029/2009GL041456.

1. Introduction

[2] Diapycnal mixing induced by oceanic internal waves is a driving force of the global thermohaline and material circulations and affects the climate. A major energy source of internal waves is tides. Diurnal tides, however, have been paid much less attention than semidiurnal tides in terms of diapycnal mixing. This may be because semidiurnal tides are dominant in most regions, and because diurnal tides are subinertial at latitudes higher than ≈30°, and hence diurnal internal tides cannot be internal waves. Nevertheless, sub-inertial diurnal tides are also important around the North Pacific rim and the Antarctic Ocean. In these regions, nearly half of the kinetic energy of barotropic diurnal tides is concentrated [*Egbert and Ray*, 2003], and diurnal tidal currents often dominate the local current field through resonant generation of topographically trapped waves [e.g., *Chapman*, 1989]. Also, with high current speed, subinertial diurnal tides can generate unsteady lee waves, which can have an intrinsic frequency higher than the local inertial frequency and hence can be internal waves [*Nakamura et al.*, 2000].

[3] In particular, numerical studies suggested that diurnal tides cause strong diapycnal mixing through the generation and breaking of large-amplitude unsteady lee waves in the Kuril Straits, located between the North Pacific and the Okhotsk Sea (Figure 1a), and that this mixing enhances the ventilation of the North Pacific intermediate layer through

the following process [*Nakamura et al.*, 2004]. First, the diapycnal mixing in the Kuril Straits causes both direct water-mass modification in the Straits and strengthened convection in the Okhotsk Sea—i.e., saline subsurface water brought up to the surface by mixing is subsequently transported by the wind-driven gyre to the northern part of the Sea, where the resulting salt flux increases the density of the Dense Shelf Water, which is produced as a result of cooling and sea-ice formation in winter and is the major source of North Pacific Intermediate Water. Second, the effects of tidal mixing are spread by a dynamical adjustment through coastally trapped waves and Rossby waves and by advective transport of heat, salt, and materials, leading to modification of the circulation and water mass properties in the North Pacific.

[4] Another reason why diapycnal mixing caused by diurnal tides is of interest is that the 18.6-year nodal cycle significantly modulates diurnal lunar tidal forces (K_1, ±14%; O_1, ±19%) [e.g., *Ray*, 2007]. The associated modulation of the barotropic tidal currents is expected to modulate the amplitude of lee waves generated, thus leading to the 18.6-year variation in the resulting mixing. Because the modulation of semidiurnal lunar tidal forces is smaller (M_2, ±4%), the effects of the 18.6-year cycle occur more significantly in regions where diurnal tides are dominant. In particular, a combination of recent studies suggests the hypothesis that the mixing due to diurnal tides in the Kuril Straits could induce 18.6-year oscillations, which are found both in the ocean and the atmosphere around the North Pacific [e.g., *Wilson et al.*, 2007], through the following process: (1) the modulation in the mixing strength causes the 18.6-year variation in the tidally enhanced ventilation process described above [*Yasuda et al.*, 2006], (2) the coastally trapped waves generated through this process reach the equator and vary the subsurface temperature there, thus regulating El Niño Southern Oscillation [*Hasumi et al.*, 2008], and (3) atmospheric teleconnections, such as the Pacific North American pattern, spread its influence [*McKinnell and Crawford*, 2007].

[5] Previous observations have found breaking events of internal waves caused by semidiurnal tides in fjords [e.g., *Farmer and Freeland*, 1983], off Hawaii [*Klymak et al.*, 2008], and off Oregon [*Nash et al.*, 2007], as well as density inversion associated with hydraulic jumps in the Strait of Gibraltar [e.g., *Wesson and Gregg*, 1994]. However, large-amplitude unsteady lee waves generated by diurnal tides and their breaking—i.e., a major mixing mechanism for subinertial diurnal tides—have not been observed in the real ocean.

[6] To look for evidence of such wave generation and breaking, observations were conducted in the Amchitka Pass, the Aleutian arc (Figure 1), where the dynamical conditions for tidally generated internal waves are similar to those in the Kuril Straits: Diurnal tides are subinertial and

[1]Pan-Okhotsk Research Center, Institute of Low Temperature Science, Hokkaido University, Sapporo, Japan.
[2]Faculty of Fisheries, Hokkaido University, Hakodate, Japan.
[3]School of Fisheries, Hokkaido University, Hakodate, Japan.
[4]Department of Earth and Planetary Science, Graduate School of Science, University of Tokyo, Tokyo, Japan.
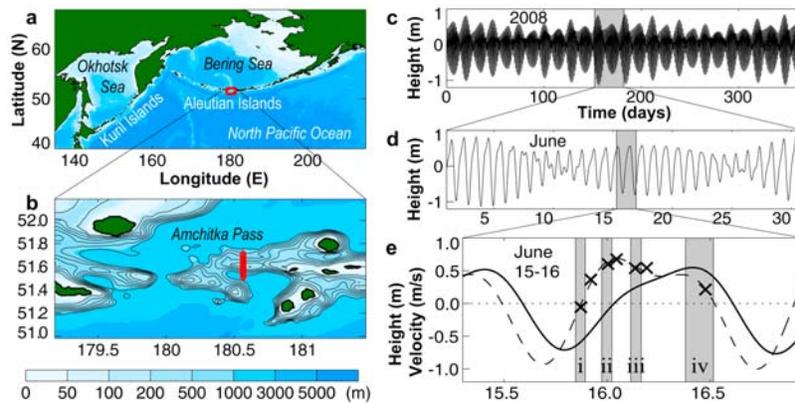
Figure 1. Locations and times of observations. Topographic maps showing (a) the location of the Amchitka Pass and (b) the observation sites in the Pass. Tidal height (TPXO7.1) in the Amchitka Pass during (c) 2008, (d) June 2008, and (e) around 16 June 2008 (UTC). Figure 1e also shows the durations of XCTD/XBT observations (shaded areas), vertically-averaged cross-ridge flow observed over the ridge top (crosses), and northward tidal velocity (dashed line) predicted based on TPXO7.1, which was lagged by -1.35 hours, amplified 1.94 times, and had a mean value of 0.055 m s^{-1} added.

dominant (Figures 1c and 1d); a ridge of ~10 km width and ~35 km length is present (Figure 1b); and the density stratification is similar in the sense that both areas are in the subarctic Pacific. In addition, mixing in the Amchitka Pass might affect the ventilation and variability around the Bering Sea and the North Pacific, as is similar to mixing in the Kuril Straits. The Pass allows a significant water exchange between the two basins [*Stabeno et al.*, 1999], which would spread the effects of mixing, and the energy flux of barotropic tides through the Pass has been estimated to increase by 36% due to the 18.6-year cycle [*Foreman et al.*, 2006]. Motivated by the observational results obtained, we then made a global estimate of the occurrence of a similar process due to the K_1 tide.

2. Observation

[7] According to numerical experiments [*Nakamura et al.*, 2000], breaking of unsteady lee waves tends to occur around the time when the barotropic tidal flow in the cross-ridge direction ceases. To estimate the time of zero cross-ridge flow, we first measured currents in the cross-ridge (i.e., meridional) section shown in Figure 1b six times, and in three of these measurements (indicated by i–iii in Figure 1e), the vertical sections of temperature and salinity were also measured. The results suggested that cross-ridge barotropic flow over the top of the ridge stops near the time of high/low water. Extensive observations were thus conducted around the time of high water (indicated by iv in Figure 1e). As it turned out, the cross-ridge barotropic flow was well correlated with a tidal model prediction (TPXO7.1 [*Egbert and Erofeeva*, 2002]) and agreed well after fitting (Figure 1e), indicating the dominance of tidal currents.

[8] The measurements were conducted using a ship-board acoustic Doppler current profiler (ADCP, Furuno Electoric CI-3500AD), 44 expendable conductivity temperature depths (XCTDs, Tsurumi-Seiki XCTD-1), and 41 expendable bathythermographs (XBTs, Tsurumi-Seiki XBT-7). The ADCP has a nominal depth range of 10–706 m with a vertical resolution of 6 m. XCTD and XBT data was visually checked for spikes, low-pass filtered, corrected for the finite-time responses of the sensors and their mismatches,

and then averaged into 1-m bins. The XBT data was further calibrated and utilized to calculate potential temperature using the adjacent XCTD data. Errors associated with the latter calculation were within 0.001°C. To exclude spurious overturns resulting from observation errors, tests of vertical and density resolutions, run length, and water mass [*Galbraith and Kelley*, 1996] were carried out with revised criteria for run length tests [*Johnson and Garrett*, 2004] and water mass tests [*Martin and Rudnick*, 2004]. The main overturn discussed below cleared all the tests.

3. Breaking Wave

[9] The extensive observations captured a breaking wave having a height of ~200 m (Figure 2a) and causing inversion of the potential density (σ_θ, hereafter referred to as density; Figure 2b). The horizontal scale of the major density inversion reached ~1.5 km with a core width of ~500 m in the cross-ridge direction. Its density ranged from 26.48 to 26.71 σ_θ (kg m^{-3}) in the meridional range of 51°34.75′–35.25′N. The breaking wave had various-scale structures and contained smaller-scale density inversions (Figures 2a and 2b), indicating the occurrence of instability and associated energy transfer from the wave to turbulent motion.

[10] The time evolution of isopycnal surfaces suggests that the breaking wave was tidal in origin (Figure 3). After the barotropic current flowed southward (leftward in Figure 3), isopycnal surfaces were lifted over the northern slope of the ridge and depressed over the southern slope (Figure 3a). As the barotropic current changed direction and flowed northward, isopycnal surfaces began to rise on the southern side and to descend on the northern side (Figure 3b). A large-amplitude elevation appeared over the ridge top as water (or the crest of the wave generated by the southward flow) crossed the ridge (Figure 3c). When the northward barotropic flow nearly ceased, internal waves generated during the northward flow grew (Figure 3d), resulting in the wave breaking shown in Figure 2. Similar wave generation was also seen over a small peak at 51°37.5′N and over a lower peak at 51°40.5′N (Figure 3e).

[11] The breaking wave had a characteristic feature of lee waves, that is, co-phase lines slanted to the upstream side
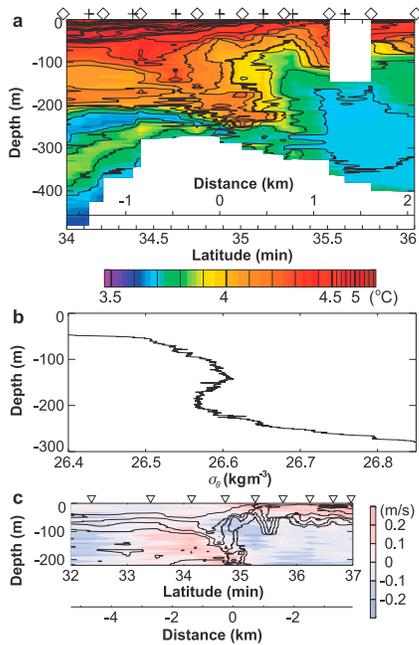
Figure 2. Breaking internal wave seen in the extensive observations (iv in Figure 1e). (a) Cross-ridge section of potential temperature and the XCTD ($\diamond$) and XBT (+) sites. White areas represent the bottom or missing data. The observations took 38 min for this whole section and 14 min for the main part of the wave (34.75′–35.5′N), during which the wave may have moved 0.2 km or less. The potential temperature behaves almost as a passive tracer in this area below the seasonal thermocline, where the density stratification is determined mostly by salinity. It was nevertheless correlated with density, except for the alternating layers located 100–300 m deep on the left hand side of the ridge top, which did not show associated density inversions of this vertical scale. (b) Vertical profile of potential density (σ_θ) at 51°35′N. (c) Cross-ridge (northward) baroclinic currents (the deviation from the vertically averaged flow over the ridge top) and the horizontal resolution of the temporally averaged ADCP data (∇). Selected isotherms are superimposed.

indicate that the breaking wave was an unsteady lee wave generated by tides.

[12] Diapycnal mixing associated with the main overturn at 51°35.0′N (Figure 2) was estimated by two approaches. One is the Thorpe scale method [e.g., *Thorpe*, 2005]. The turbulence dissipation rate was estimated as $\varepsilon \approx cN_s^3 L_T^2$, where $c \sim 1$, N_s is the mean sorted buoyancy frequency, and L_T is the Thorpe scale. The diapycnal diffusivity coefficient, κ_ρ, was then estimated as $\kappa_\rho = \gamma \varepsilon / N_s^2$, where the conventional value of γ is 0.2. This approach yields κ_ρ of 1.5 m^2 s^{-1} with calculated values of L_T (60 m), N_s (0.0021 rad s^{-1}), and ε (3.1 × 10^{-5} W kg^{-1}). The other approach assumed that the statically unstable region will be vertically mixed, following past numerical experiments [e.g., *Scinocca and Peltier*, 1993]. Equating the resulting density flux to a vertical diffusive flux, $\kappa_z \partial \rho_s / \partial z$ where ρ_s is sorted density, we obtain a vertical diffusivity coefficient, κ_z, that almost corresponds to κ_ρ. Here, the density flux was estimated as the density transport divided by the time required for mixing,
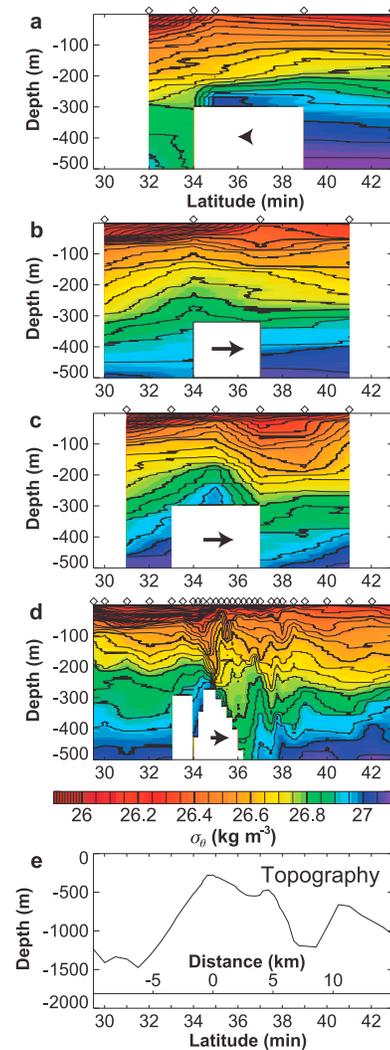

Figure 3. (a–d) Temporal evolution of potential density surfaces. The observation times of Figures 3a, 3b, 3c, and 3d are shown by shaded areas numbered i, ii, iii, and iv in Figure 1e, respectively. Arrows show the direction of barotropic cross-ridge flow at the ridge top. (e) The measured bottom topography.
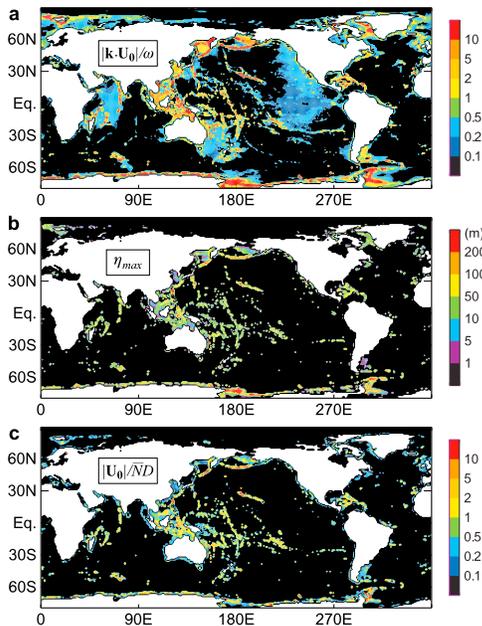
(i.e., south), as seen in both current and density fields (Figures 2c and 3d). In fact, the ratio of the Doppler shift (or lee wave frequency) to tidal frequency (kU/ω) was estimated to be 11, suggesting that the wave was an unsteady lee wave [*Nakamura et al.*, 2000], where U, ω, and k are barotropic tidal flow speed, tidal frequency, and horizontal wavenumber estimated from Figure 2. Also, the intrinsic frequency estimated from the dispersion relation (8 × 10^{-4} rad s^{-1}) roughly agreed with the lee wave frequency ($kU \approx 7.9 × 10^{-4}$ rad s^{-1}). Actually, the observed time evolution had similarities to those of unsteady lee waves seen in numerical experiments [*Nakamura et al.*, 2000]. In addition, the inverse Froude number ($\overline{N}\eta/U$) and the wave Froude number ($U/\overline{N}D$) were estimated to be 3 and 0.2, respectively, where $\overline{N}$ is the depth average of buoyancy frequency, and D is the water depth at the ridge top, and wave height, η, was used instead of topographic height because the tidal excursion is finite. The two estimated numbers suggest that the wave generating force was strong enough for the wave to break but that the flow was not hydraulically controlled [e.g., *Baines*, 1995]. All of these

Figure 4. (a) The condition for lee-wave generation ($|\mathbf{k} \cdot \mathbf{U_0}|/\omega$), (b) maximum possible wave height (η_{max}), and (c) the condition for hydraulic jump ($|\mathbf{U_0}|/\overline{N}D$) for the K_1 tide. Here, $|\mathbf{k} \cdot \mathbf{U_0}|/\omega$ and η_{max} are set to zero, where $N_\lambda \leq |\mathbf{k} \cdot \mathbf{U_0}|/\omega$. The calculation used ETOPO1 bathymetric data, TPXO7.1 tidal data, and density data ($\sigma_0, \sigma_2, \sigma_4$) of WOCE Global Hydrographic Climatology [*Gouretski and Koltermann*, 2004]. Abnormal values found in the last in some marginal seas were corrected. The calculation was conducted on $1' \times 1'$ grids and maximum values in $1° \times 1°$ boxes are shown.

where the density transport was calculated as the vertical integration of the magnitude of the difference between the density observed and the density that would be achieved by vertical mixing to a statically stable state. This approach gave κ_z of 1.2 m^2 s^{-1} when mixing occurred in the mean buoyancy period ($2\pi/N_s$) of 3000 s.

[13] Both approaches gave diffusivity $\sim 10^4$ times larger than typical values found in the open oceans. (The estimates yield a temporal average of 0.08–0.1 m^2 s^{-1} if the mixing lasts for the buoyancy period and occurs twice a day, while observational estimates are $\sim 0.1 \times 10^{-4}$ m^2 s^{-1} away from topographic features or at latitudes higher than $\approx 30°$ or lower than $\sim 15°$ [e.g., *Gregg et al.*, 2003; *Hibiya et al.*, 2006].) The rough agreement of the two estimates together with the wide applicability of the Thorpe scale method [*Wesson and Gregg*, 1994] supports these estimates, though the estimates should have a margin of error.

4. Global Distribution

[14] Figure 4a shows values of $|\mathbf{k} \cdot \mathbf{U_0}|/\omega$ estimated for the largest diurnal constituent, the K_1 tide, where lee wave generation is expected when $|\mathbf{k} \cdot \mathbf{U_0}|/\omega \geq 1$ and $N_\lambda > |\mathbf{k} \cdot \mathbf{U_0}|$. Here, $\mathbf{U_0}$ is the amplitude vector of horizontal, barotropic tidal velocity, ω is the corresponding tidal frequency, and N_λ is buoyancy frequency averaged from the bottom in one vertical wavelength of hydrostatic lee waves ($2\pi(|\mathbf{k} \cdot \mathbf{U_0}|/|\mathbf{k}|)/N_\lambda$ [e.g., *Baines*, 1995]). Horizontal wavenumber

vector, $\mathbf{k}$, was estimated from the horizontal scale of the vertical velocity amplitude ($W_0 = -\mathbf{U_0} \cdot \nabla D$, where D is depth). Note that lee wave generation is likely to be underestimated particularly in areas of weak tidal currents, because of the horizontal resolution ($1' \times 1'$) of the topographic data used (ETOPO1 [*Amante and Eakins*, 2008]). For $|\mathbf{U_0}| \sim 0.01$ m s^{-1}, the condition $|\mathbf{k} \cdot \mathbf{U_0}|/\omega \geq 1$ requires a topographic length scale of less than 1 km, which is hardly resolved because $1'$ in latitude is 1.852 km.

[15] The global map suggests that lee waves are expected in other regions along the Aleutian and Kuril Islands, and also around the Antarctic and Pacific Oceans. The generation condition is also met in the Indian Ocean, the Indonesian Seas, the northwest of Canada, and around the Caribbean and Svalbard Islands.

[16] As a rough measure of the significance of the lee wave process, an upper limit of the wave height of tidally generated lee waves (η_{max}) was estimated together with the Froude number ($|\mathbf{U_0}|/\overline{N}D$; Figures 4b and 4c). The upper limit was estimated as the minimum of the vertical excursion of barotropic tidal flow estimated at a fixed point ($2|W_0|/\omega$), the depth (D), the height of topographic features (ΔH), and a half vertical wavelength ($\lambda_z/2$). This is based on two facts: (1) the maximum vertical displacement of isopycnal surfaces (i.e., wave height) is nearly equal to the maximum vertical excursion of the fluid moving with the flow, which is less than or equal to min($2|W_0|/\omega$, D, ΔH) in a Boussinesq fluid; and (2) the wave height of internal waves should be less than or comparable to $\lambda_z/2$, as long as the wave ray slope is small and the horizontal scale of the density inversion is smaller than the horizontal wavelength. Here, λ_z was approximated as the vertical wavelength of hydrostatic lee waves ($2\pi(|\mathbf{k} \cdot \mathbf{U_0}|/|\mathbf{k}|)/N_\lambda$). ΔH was estimated as $\Delta H = \max(H') - \min(H')$, where H' is the deviation of topographic height (H) from the topographic mean slope ($H' = H - \mathbf{l} \cdot \overline{\nabla H}$, where the overbar denotes the horizontal average and $\mathbf{l}$ is horizontal displacement). The calculations for ΔH and H' were performed within the distance of the local horizontal tidal excursion from each point.

[17] Estimated values of η_{max} exceed 100 m along the Aleutian and Kuril Islands, and around the Pacific and Antarctic Oceans, particularly around the Ross and Weddell Seas. The distribution is similar to that of $|\mathbf{k} \cdot \mathbf{U_0}|/\omega$, but is more concentrated in areas of a sharp change in depth, such as shelf breaks, ridges, and seamounts. The distribution of the Froude number is quite similar to that of η_{max}. In regions of strong tidal currents (e.g., the Kuril and Aleutian Islands), areas having large η_{max} are interwoven with areas where the jump condition is met ($|\mathbf{U_0}|/\overline{N}D > 1/\pi$). Vigorous mixing might be caused in such areas by the K_1 tide, though estimation of the mixing strength needs future work.

[18] In contrast to the K_1 case, η_{max} for the M_2 tide, the largest semidiurnal constituent, is insignificant around the Antarctic, except for the Weddell Sea, but is significant in the Atlantic Ocean, according to the map of W_0 calculated by *Legg and Klymak* [2008].

5. Summary and Discussion

[19] This study showed evidence that subinertial tides are causing vigorous diapycnal mixing through the breaking of unsteady lee waves in the real ocean. This process is fundamental to the tidally enhanced ventilation and the tidally

induced bi-decadal oscillation around the North Pacific. We also made global maps of the areas where lee waves or hydraulic jumps are expected. These revealed further implications: (1) Mixing due to lee waves might be significant for a global estimate of diapycnal mixing because such areas are distributed globally. (2) Diurnal tides could affect the formation of the Antarctic Bottom Water (AABW) through the generation of lee waves or hydraulic jumps, which is expected around the Ross and Weddell Seas, two of the major sources of the AABW. (3) The 18.6-year variation could be significant in areas having a large Froude number or η_{max}. (4) The combination of the last two suggests the possibility that the 18.6-year cycle could affect the formation of the AABW. A quantitative understanding of these possible effects would be obtained from a global estimate of diapycnal mixing caused by lee wave breaking (and jumps), although problems concerning nonlinearity of waves and tidal currents still remain, and higher resolution data of the topography, tides, and stratification are desired.

References

Amante, C., and B. W. Eakins (2008), *ETOPO1 1 Arc-Minute Global Relief Model: Procedures, Data Sources and Analysis*, http://www.ngdc.noaa.gov/mgg/global/global.html, Natl. Geophys. Data Cent., Boulder, Colo.

Baines, P. G. (1995), *Topographic Effects in Stratified Flow*, Cambridge Univ. Press, New York.

Chapman, D. C. (1989), Enhanced subinertial diurnal tides over isolated topographic features, *Deep Sea Res., Part A*, *36*(6), 815–824.

Egbert, G. D., and R. D. Ray (2003), Semi-diurnal and diurnal tidal dissipation from TOPEX/Poseidon altimetry, *Geophys. Res. Lett.*, *30*(17), 1907, doi:10.1029/2003GL017676.

Egbert, G. D., and S. Y. Erofeeva (2002), Efficient inverse modeling of barotropic ocean tides, *J. Atmos. Oceanic Technol.*, *19*(2), 183–204.

Farmer, D. M., and H. J. Freeland (1983), The physical oceanography of fjords, *Prog. Oceanogr.*, *12*, 147–220.

Foreman, M. G. G., P. F. Cummins, J. Y. Cherniawsky, and P. Stabeno (2006), Tidal energy in the Bering Sea, *J. Mar. Res.*, *64*, 797–818.

Galbraith, P. S., and D. E. Kelley (1996), Identifying overturns in CTD profiles, *J. Atmos. Oceanic Technol.*, *13*, 688–702.

Gouretski, V. V., and K. P. Koltermann (2004), *WOCE Global Hydrographic Climatology*, Ber. Bundesamtes Seeschifffahrt Hydrogr. 35, Hamburg, Germany.

Gregg, M. C., T. B. Sanford, and D. P. Winkel (2003), Reduced mixing from the breaking of internal waves in equatorial waters, *Nature*, *422*, 513–515.

Hasumi, H., I. Yasuda, H. Tatebe, and M. Kimoto (2008), Pacific bidecadal climate variability regulated by tidal mixing around the Kuril Islands, *Geophys. Res. Lett.*, *35*, L14601, doi:10.1029/2008GL034406.

Hibiya, T., M. Nagasawa, and Y. Niwa (2006), Global mapping of diapycnal diffusivity in the deep ocean based on the results of expendable current profiler (XCP) surveys, *Geophys. Res. Lett.*, *33*, L03611, doi:10.1029/2005GL025218.

Johnson, H. L., and C. Garrett (2004), Effects of Noise on Thorpe scales and run lengths, *J. Phys. Oceanogr.*, *34*, 2359–2372.

Klymak, J. M., R. Pinkel, and L. Rainville (2008), Direct breaking of the internal tide near topography: Kaena Ridge, Hawaii, *J. Phys. Oceanogr.*, *38*, 380–399.

Legg, S., and J. Klymak (2008), Internal hydraulic jumps and overturning generated by tidal flow over a tall steep ridge, *J. Phys. Oceanogr.*, *38*, 1949–1964.

Martin, J. P., and D. L. Rudnick (2004), Inferences and observations of turbulent dissipation and mixing in the upper ocean at the Hawaiian Ridge, *J. Phys. Oceanogr.*, *37*, 476–494.

McKinnell, S. M., and W. R. Crawford (2007), The 18.6-year lunar nodal cycle and surface temperature variability in the northeast Pacific, *J. Geophys. Res.*, *112*, C02002, doi:10.1029/2006JC003671.

Nakamura, T., T. Awaji, T. Hatayama, K. Akitomo, T. Takizawa, T. Kono, Y. Kawasaki, and M. Fukasawa (2000), The generation of large-amplitude unsteady lee waves by subinertial K1 tidal flow: a possible vertical mixing mechanism in the Kuril Straits, *J. Phys. Oceanogr.*, *30*, 1601–1621.

Nakamura, T., T. Toyoda, Y. Ishikawa, and T. Awaji (2004), Tidal mixing in the Kuril Straits and its impact on ventilation in the North Pacific Ocean, *J. Oceanogr.*, *60*, 411–423.

Nash, J. D., M. H. Alford, E. Kunze, K. Martini, and S. Kelly (2007), Hotspots of deep ocean mixing on the Oregon continental slope, *Geophys. Res. Lett.*, *34*, L01605, doi:10.1029/2006GL028170.

Ray, R. D. (2007), Decadal climate variability: Is there a tidal connection?, *J. Clim.*, *20*, 3542–3560.

Scinocca, J. F., and W. R. Peltier (1993), The instability of Long's stationary solution and the evolution toward severe downslope windstorm flow. Part I: Nested grid numerical simulations, *J. Atmos. Sci.*, *50*, 2245–2263.

Stabeno, P. J., J. D. Schumacher, and K. Ohtani (1999), The physical oceanography of the Bering Sea, in *Dynamics of the Bering Sea*, pp. 1–28, Univ. of Alaska Sea Grant, Fairbanks, Alaska.

Thorpe, S. A. (2005), *The Turbulent Ocean*, Cambridge Univ. Press, New York.

Wesson, J. C., and M. C. Gregg (1994), Mixing at Camarinal sill in the Strait of Gibraltar, *J. Geophys. Res.*, *99*, 9847–9878.

Wilson, R., G. Wiles, R. D'Arrigo, and C. Zweck (2007), Cycles and shifts: 1300 years of multi-decadal temperature variability in the Gulf of Alaska, *Clim. Dyn.*, *28*, 425–440, doi:10.1007/s00382-006-0194-9.

Yasuda, I., S. Osafune, and H. Tatebe (2006), Possible explanation linking 18.6-year period nodal tidal cycle with bi-decadal variations of ocean and climate in the North Pacific, *Geophys. Res. Lett.*, *33*, L08606, doi:10.1029/2005GL025237.

M. Nagasawa, Department of Earth and Planetary Science, Graduate School of Science, University of Tokyo, Tokyo 113-0033, Japan.

T. Nakamura and H. Mitsudera, Institute of Low Temperature Science, Hokkaido University, Sapporo 060-0819, Japan. (nakamura@lowtem.hokudai.ac.jp)

Y. Isoda, Faculty of Fisheries, Hokkaido University, Hakodate 041-8611, Japan.

S. Takagi, School of Fisheries, Hokkaido University, Hakodate 041-8611, Japan.